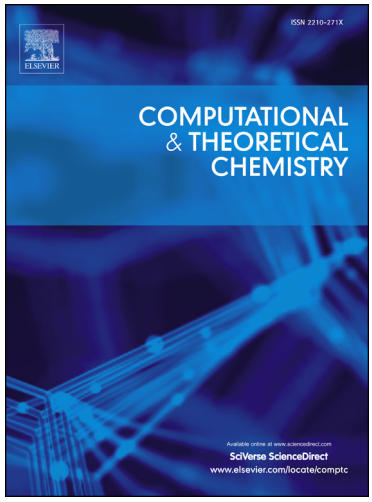

New insights on lithium-cation microsolvation by solvents forming hydrogen-bonds: water *versus* methanol

J.L. Llanio-Trujillo, J.M.C. Marques, F.B. Pereira

PII: S2210-271X(13)00280-6
DOI: http://dx.doi.org/10.1016/j.comptc.2013.06.043
Reference: COMPTC 1169

To appear in: *Computational & Theoretical Chemistry*

Received Date: 18 May 2013
Revised Date: 25 June 2013
Accepted Date: 27 June 2013

Please cite this article as: J.L. Llanio-Trujillo, J.M.C. Marques, F.B. Pereira, New insights on lithium-cation microsolvation by solvents forming hydrogen-bonds: water *versus* methanol, *Computational & Theoretical Chemistry* (2013), doi: http://dx.doi.org/10.1016/j.comptc.2013.06.043

New insights on lithium-cation microsolvation by solvents forming hydrogen-bonds: water *versus* methanol

J. L. Llanio-Trujillo[a], J. M. C. Marques[a,*], F. B. Pereira[b]

[a] *Departamento de Química, Universidade de Coimbra, 3004-535 Coimbra, Portugal*
[b] *Instituto Superior de Engenharia de Coimbra, Quinta da Nora, 3030-199 Coimbra, Portugal, and Centro de Informática e Sistemas da Universidade de Coimbra (CISUC), 3030-290 Coimbra, Portugal*

Abstract

This investigation uses a recent methodology, essentially based on our evolutionary algorithm (EA) to get new insights about the energetics and structure of the first solvation shells of lithium ion in polar solvents that form important hydrogen bonds. We employed the EA to search for the low-energy structures of the $Li^+(H_2O)_n$ and $Li^+(CH_3OH)_n$ clusters (with $n \leq 20$) as modeled by commonly used rigid nonpolarizable force-field potentials. Particular emphasis is given to the characterization of the putative global minima; for $Li^+(CH_3OH)_{17}$, the EA discovered a new global minimum with five water molecules directly coordinating the ion. Smaller-size clusters were, then, re-optimized by employing electronic structure methods, namely, DFT (with the B3LYP functional and both the 6-31+G* and 6-311+G** basis sets) and MP2 (with the aug-cc-pVDZ basis set). In the case of $Li^+(H_2O)_n$, the *ab initio* global minimum structures are similar to those obtained with the EA up to $n = 10$. However, for $n = 17$, the structure of the global minimum discovered by the EA is different from the lowest-energy cluster obtained after re-optimization at the MP2/aug-cc-pVDZ level of theory. Such energy reorder may be attributed to the water-water interaction. As for the $Li^+(CH_3OH)_n$ clusters, the re-optimization process leads more often to a reorder in the energy of the minimum structures. Thus, for fluxional clusters like the $Li^+(CH_3OH)_n$ ones that show a huge number of stationary configurations within a small energy window, it is mandatory to carefully choose various structures, besides the global minimum, to be re-optimized at the *ab initio* or DFT levels. Due to the difficulty on choosing adequate departing structures by the usually employed chemical intuition, we noticed that some low-energy minima (including the global one) of even small $Li^+(CH_3OH)_n$ clusters were missed in literature. We showcase this problem in the $Li^+(CH_3OH)_6$ cluster, whose vibrational frequencies in the C-O stretching region and corresponding infrared intensities were calculated at the DFT level of theory and compared with previously reported results.

Keywords: Li^+ microsolvation, water, methanol, hydrogen bonds, evolutionary algorithms, electronic structure calculations, spectrum

*Corresponding author
Email addresses: llanio.jorge@gmail.com (J. L. Llanio-Trujillo), qtmarque@ci.uc.pt (J. M. C. Marques), xico@dei.uc.pt (F. B. Pereira)

1. Introduction

The study of the immediate molecular environment around solvated metal ions, primarily focused on the condensed-phase, has drawn much attention from both experimental and theoretical sides. More recent advances in ion sources and laser technology have spurred further investigations on this challenging research topic, with special emphasis on elucidating the structure and vibrational spectra in gas-phase (see Refs. [1–5] and references therein). Such research work is of great significance as its results may benefit other fields of knowledge currently seeking molecular-level understanding on ion solvation to develop their own models. Among several examples reported in the literature, we mention the importance of Li^+ solvation in the context of the development of lithium-ion batteries [6], as well as in the study of the binding mechanism of ions to biomolecules and selective ion permeation through narrow channel proteins in biological sciences [7].

Similarly, atomic and molecular clusters are usually viewed as a bridge across disciplines [8], since they have also attracted the attention of many researchers from several areas over the last decades. Such interest in cluster systems is mainly due to a marked variation of their properties with size. Indeed, clusters may be regarded as intermediate entities exhibiting size-dependent chemical and physical properties that connect the single atom or molecule with the corresponding bulk phase. Thus, by adding step-wise solvent molecules to the solute, it is possible to acquire a molecular-level perception of the solvation phenomena. From the theoretical point of view, the study of microsolvation of ionic species takes advantage of using state of the art optimization methods for discovering low-energy structures of the clusters formed by both the solute and the solvent molecules. According to this endeavor, we have developed in the last years unbiased evolutionary algorithms (EAs) that seek the global minimum structure of atomic [9–13] and molecular [14] clusters; these algorithms have been successfully applied to discover the global minimum of several atomic and molecular aggregates (see Refs. [15, 16] and references therein). Clearly, EAs are among the best methods for global geometry optimization of clusters, and they are known to over perform random search algorithms, like the so-called big-bang method [17], as we have shown in a recent work [18, 19].

Water is by far the most used solvent due to its abundance and chemical properties. A special role in the solvation phenomena is played by the large dipole moment of water, as well as its ability to establish hydrogen bonds. In particular, the relevance of the hydrogen-bond network to state the most stable structure in water clusters has been assessed by several authors [20–24]. Similar to water, methanol is another polar solvent exhibiting hydrogen-bond networks. Hence, $(CH_3OH)_n$ clusters have been extensively studied in the literature [25–29]. In turn, water and methanol are frequently used as solvents in studies of microsolvation involving alkali ions. Microhydration of alkali ions has been studied by employing global optimization methods. Specifically, Hartke and collaborators [30–33] have used their own EA [34, 35] to carry out a detailed investigation on the structural properties of $Na^+(H_2O)_n$, $K^+(H_2O)_n$, and $Cs^+(H_2O)_n$ clusters, while Wales and co-workers [36] have obtained putative global minimum geometries of $Li^+(H_2O)_n$ (for $n \leq 20$). Also, the microsolvation of alkali-ions with methanol molecules have drawn the attention of several authors [32, 37–41]. In particular, García-Muruais *et al.* [39] performed a computational analysis of $Li^+(CH_3OH)_n$ ($n = 1-5$) at different levels of theory with the $6-31G^*$ basis set and concluded that the first solvation shell of the metal-ion is saturated with four methanol molecules.

In turn, Wu *et al.* [40] used electrospray ionization (ESI) as an ion source to produce $Li^+(CH_3OH)_n$ ($n = 1 - 10$) clusters for further infrared spectroscopic measurements in the C-O stretching region, and observed a gradual blue shift of the corresponding frequency as n increased from 5 to 10, thus experimentally supporting the formation of a second solvation shell at $n = 5$ in this system. At the same time, based on the comparison of their experimental and DFT/B3LYP(6-31+G*) calculated infrared spectra, those authors [40] made an additional effort to identify the structural features of $Li^+(CH_3OH)_n$ clusters for $n = 5 - 7$.

In a recent work [16], we have investigated the microsolvation of alkali-ions in nonpolar environments associated to aromatic rings. Specifically, we have employed an EA to discover putative global minima of clusters of Na^+, K^+, or Cs^+ solvated with up to $n = 21$ benzene molecules. The global intermolecular interaction was separated into benzene-benzene and ion-benzene contributions, using a potential model based on different decompositions of the molecular polarizability of benzene [42]. The electrostatic component ensures the model to accurately describe both the cation quadrupole and the quadrupole-quadrupole interactions at long-range distances, while the non-electrostatic part is given as a sum of pair-potentials (of two or three-body type) that are represented by improved Lennard-Jones functions [43, 44]. We have concluded from this study [16] that the first solvation shell may allocate three (for Na^+) or four (for K^+ and Cs^+) benzene molecules, and its structure keeps essentially unchanged as more solvent molecules are added to the cluster. In turn, we have observed that "structure-breaking" effect on benzene is larger for the smaller cations (*e.g.*, Na^+), which is in the same line as the findings obtained in the microsolvation of alkali-ions with water molecules [36, 45].

The present work is committed with the microsolvation study of another alkali-ion, *i.e.*, Li^+, in polar solvents that form important hydrogen bonds. The microsolvation of Li^+ with water is revisited, while putative global minima for $Li^+(CH_3OH)_n$ ($n = 1 - 20$) are obtained for the first time; both electronic structure calculations and commonly used non-polarizable empirical representations for the interaction potential have been employed. Besides the theoretical study of the energetics and structural properties of $Li^+(H_2O)_n$ and $Li^+(CH_3OH)_n$ clusters, we also aim to test the performance of our EA in discovering the global minimum geometry of such kind of systems. This is accomplished by comparing our results for the $Li^+(H_2O)_n$ clusters with those of González *et al* [36] that are available from the Cambridge Cluster Database [46].

The plan of the paper is as follows. In Section 2, we present the interaction potential which has been used to model the $Li^+(H_2O)_n$ and $Li^+(CH_3OH)_n$ clusters. Also described in Section 2 are the EA employed in the global geometry optimization and the electronic structure calculations performed for the $Li^+(H_2O)_n$ and $Li^+(CH_3OH)_n$ clusters. The main results are presented and discussed in Section 3. Finally, the main conclusions are gathered in Section 4.

2. Computational methods

2.1. Interaction potential models

The total interaction potential, $V_{\rm cluster}$, for both types of clusters, that is $Li^+(H_2O)_n$ and $Li^+(CH_3OH)_n$, was modeled as

$$V_{\rm cluster} = V_{\rm solvent-solvent} + V_{\rm ion-solvent} \quad (1)$$

where the two terms represent the solvent-solvent (water-water or methanol-methanol) and Li^+-solvent interactions, respectively. The solvent-solvent term is composed by a sum of inter-monomer pair-potentials, where the electrostatic interaction is described by the Coulomb law and the dispersion-repulsion component is represented by a Lennard-Jones 12-6 function: in a pairwise additive manner involving inter-monomer pairs of sites:

$$V_{\text{solvent}-\text{solvent}} = \sum_{J<K}^{n} \sum_{\substack{j\in J \\ k\in K}}^{n_s} \left\{ \frac{q_j q_k}{r_{jk}} + 4\,\epsilon_{jk} \left[\left(\frac{\sigma_{jk}}{r_{jk}} \right)^{12} - \left(\frac{\sigma_{jk}}{r_{jk}} \right)^{6} \right] \right\} \tag{2}$$

In Eq. (2), n_s designates the total number of sites in each solvent molecule (*i.e.*, monomer), and j and k represent the interaction sites localized on monomers J and K, respectively; r_{jk} is the inter-site distance, whereas ϵ, σ and q are parameters that must be specified for each jk-interaction. In the case of water, we have employed the extensively used four-site ($n_s = 4$) TIP4P potential [47], while the methanol-methanol interaction was represented by the six-site ($n_s = 6$) OPLS-AA model [48]. In a similar way, the ion-solvent component of Eq. (1) is also modeled by a sum of pair-potentials involving Coulomb and LJ potential terms like in Eq. (2), but the summation runs, now, over all interactions between the Li^+ ion and the sites of the whole set of monomers.

It is worth noting that the TIP4P model [47] employs a single LJ site which coincides with the oxygen atom at each water molecule, while the three charge-sites are located at the two hydrogens and at a distance of 0.15 Å from the O-atom, along the bond-angle bisectrix. Conversely, in the OPLS-AA model [48], both LJ and charge sites coincide at the positions of the six atoms of the methanol molecule, which is kept fixed in its equilibrium geometry. The parameters for the ion-water LJ function were obtained by using the values of Dang [49] for Li^+ and the Lorentz-Berthelot combining rules. As for ion-methanol, the calculation of all the parameters for the six LJ functions was achieved by employing the geometric mean between σ_{Li^+} (or ϵ_{Li^+}) and the corresponding value for similar site-site interaction of two methanol molecules. In turn, the σ_{Li^+} and ϵ_{Li^+} parameters were computed by using the relations

$$\sigma_{Li^+} = \sqrt[6]{\frac{A_I^2}{B_I^2}} \tag{3}$$

$$\epsilon_{Li^+} = \frac{B_I^4}{4\,A_I^2} \tag{4}$$

where A_I and B_I are the van der Waals parameters estimated for Li^+ by Åqvist [50].

2.2. Evolutionary algorithm

The global energy minima were located using our own evolutionary algorithm (EA). It is worth noting that this algorithm has shown [14] to be reliable for discovering the minimum energy structure of clusters of water (up to 20 molecules), benzene (up to 30 molecules), and cation benzene (up to 20 molecules). More recently, it has been also applied for the study of alkali-ions (*i.e.*, Na^+, K^+, and Cs^+) microsolvation with up to 21 benzene molecules [16]. Since it was already fully detailed in the original paper [14], here we just highlight the most relevant features of the optimization method. The EA randomly generates several initial

solutions and then iteratively applies selection and genetic operators to seek for configurations with the lowest potential energy. The clusters are represented by fixing the lithium-cation at the geometric center of a 3D cube with edge length of 12 Å. Then, each solution encodes the location of the N solvent particles by maintaining N six-tuples of the form: $(x_i, y_i, z_i, \alpha_i, \beta_i, \gamma_i)$. The first three variables define the Cartesian coordinates of the i-th particle center of mass, while the remaining three specify the corresponding Euler angles. All solutions belonging to the EA populations are local minima. To accomplish this, initial random clusters and aggregates resulting from the application of genetic operators (see details below) are relaxed until convergence to the nearest local optimum. L-BFGS [51], a quasi-Newton gradient driven local optimization procedure was selected for this task.

The EA operates as a fully generational architecture and, therefore, in every iteration the whole set of solutions is replaced. Three steps are applied to create a new generation:

1. Selection: The most promising clusters belonging to the current population, *i.e.*, the ones with the lower potential energy, are chosen as parents to bias the formation of the next set of solutions. Stochastic tournament selection is the operator applied in this step.
2. Crossover: Selected parents are randomly paired and exchange components, leading to the appearance of new aggregates. In the EA described in this work, we rely on simulated binary crossover [52], a state-of-the-art arithmetic operator that has been successfully applied in cluster geometry optimization problems [14, 16].
3. Mutation: Sigma mutation is applied to the clusters that result from crossover and slightly modifies the coordinates and/or orientation of a few solvent molecules. Mutated variables are updated with values drawn from a Gaussian distribution with mean 0 and standard deviation $\sigma = 0.1$.

After local optimization, the obtained solutions are evaluated and a new generation starts until a predetermined number of iterations is achieved. To prevent the disappearance of the best solution from one generation to the other, the EA contains an elitist operator. The optimization method offers the option to keep trace of a pool of local minima using energetic and structural similarity selection criteria. However, in the present study, rather than to attempt an exhaustive and systematic search of all minima for each cluster-number n, we have chosen to focus ourselves on the identification of the lowest energy conformations, mainly, global energy minima (GM). A number of preliminary tests allowed us to determine a robust EA setting that was adopted in all the calculations described in the next section: Number of runs: 30; Evaluations per run: 100000; Population size: 100; Tourney size: 5; Crossover rate: 0.75; Mutation rate: 0.1.

2.3. Electronic structure calculations

Cluster geometry electronic-structure optimizations and frequency calculations were performed using second-order Möller-Plesset perturbation (MP2) within the frozen-core approximation (note that then, Li^+ has only 1s core with no valence electrons to correlate) and density funtional theory (DFT) methods as implemented in GAMESS program [53]. The largest component of the gradient was required to be less than $1.0 \times 10^{-5}\,\mathrm{E_h\,a_0^{-1}}$. The calculations carried out at the MP2

level employed the double-ζ quality correlation consistent, polarized valence (cc-pVDZ) basis set for Li via Basis Set Exchange [54], with additional diffuse functions (aug-cc-pVDZ [55, 56]) basis sets for water and methanol; in addition, single-point MP2/aug-cc-pVTZ calculations were also carried out for some structures that have been optimized at the less expensive MP2/aug-cc-pVDZ level of theory. The DFT calculations were performed with the Becke three parameter hybrid functional coupled with the Lee-Yang-Parr correlation functional (B3LYP [57, 58]) and the 6-31+G* and 6-311+G** basis sets [53].

3. Results and discussion

This section is divided in two parts. First, the microsolvation of Li^+ by water, already treated in the same context by González *et al.* [36], is revisited here to test the reliability of the EA for searching the global minimum structures of this kind of clusters. Second, we report putative global minimum structures of $Li^+(CH_3OH)_n$ (with $n \leq 20$), as modeled with the OPLS-AA semiempirical potential described in Section 2, that were obtained with the EA, and such results are compared with the corresponding ones for $Li^+(H_2O)_n$ clusters. Moreover, by departing from some of the low-energy structures of both $Li^+(H_2O)_n$ and $Li^+(CH_3OH)_n$, we have further optimized the geometry of the smallest clusters by employing *ab initio* and/or DFT methods. The geometry of all optimized structures are available from the authors upon request and the corresponding mol files can be downloaded from the present online article.

As we are dealing with the lithium cation surrounded by polar solvent molecules that can form hydrogen-bonds, both electrostatic and H-bonding noncovalent long-range interactions are simultaneously present in these systems. Thus, the lowest-energy structure of each cluster will result from the competition (or cooperation) of those components of the interaction. In addition, due to sterical repulsion between neighboring methyl groups, the formation of methanol H-bonded networks are expected to show extra difficulty in comparison with the water ones. In fact, the presence of CH_3 groups in methanol disturbs the ordered H-bonded network that can be found in water clusters.

3.1. $Li^+(H_2O)_n$ clusters

In a previous work, González *et al.* [36] reported putative global minima of $Li^+(H2O)_n$ clusters for $n \leq 20$, that were located with the basin-hopping algorithm [59]. Taking such minima as reference, we aim to test our EA by employing the same potential function as in Ref. [36]. Then, the global minima obtained with the EA are compared with the corresponding reference structures [36], as reported in the Cambridge Cluster Database [46] (CCD). The main results of the comparison are shown in Table 1. Concerning the energy of the clusters, it is clear from Table 1 that, in general, one obtains global minima with the EA that are slightly deeper than the corresponding ones in the CCD (*i.e.*, $\Delta E < 0$); the only exceptions are for $n = 1$, 2, and 3. Since the values of ΔE are always very small (*i.e.*, less than 1 kJ mol^{-1}), the energetic criterion should be complemented with a structural comparison to decide whether a new global minimum has been located.

The structural comparison of clusters has been carried out by means of the SAICS program [60] (free available from [61]), which is able to distinguish between enantiomer structures. In fact, enantiomers are commonly appearing within low-symmetry minima during the optimization process and they cannot be identified

by an energetic criterion, because such specular-image structures correspond to the same point in the potential energy surface. In addition, SAICS is appropriate to compare chemical structures resulting from optimization procedures that may reorder the atoms or molecules (like in the EAs), since it applies the Hungarian algorithm [62, 63] to get the right order of the particles. In Table 1, we show that the root mean square deviation (RMSD) obtained after the best overlap of the two structures with SAICS program is usually very small (*e.g.*, 1.0×10^{-3} Å for $n = 11$), which is a clear evidence of the success of the EA in discovering the global minima. For some instances, however, the best overlap is only reached with the mirror-image structure (whose RMSD values are given in square brackets) and, hence, it indicates that the EA discovered an enantiomer of the global minimum reported in the CCD. A different situation occurs for $n = 17$, whose the structure resulting from the optimization with the EA, as well as its mirror-image, cannot overlap the corresponding one given in the CCD. The best overlap leads to a RMSD of 1.22 Å, which points out to the discovery of a new global minimum of $Li^+(H_2O)_{17}$ with the EA; further discussion on the structure and energetics of the new minimum for $n = 17$ is given in the end of this subsection.

We also give in Table 1 the success rate of the EA (*i.e.*, percentage of runs where the putative global minimum was found). It is clear that the success rate is notably high for up to $n = 13$, which is similar to the corresponding result obtained with the same EA for water clusters [14]. Since the complexity of the energy landscape increases with n, the success rate tends to decrease for larger clusters; particular difficult to discover are the global minima for $n = 18$ and 20, whose success rates become less of 15%. However, the new global minimum for $n = 17$ was reached by the EA in 6 runs out of 30.

In order to investigate the reliability of the semi-empirical potential model employed in the geometry optimization with the EA, we have re-optimized the first ten global minima structures by employing the MP2 *ab initio* method with the aug-cc-pVDZ basis set. All the *ab initio* structures are in good agreement with the departure geometries (*i.e.*, the global minimum ones for the semi-empirical potential), which is shown by the almost coincidence of $O - Li^+$ distances in Figure 1; accordingly, the two lines linking the corresponding average distances are also essentially coincident. Moreover, the MP2/aug-cc-pVDZ optimized structures for the $Li^+(H_2O)_n$ clusters (with $1 \leq n \leq 6$) are in reasonable agreement with other reports [64–67] that used different levels of theory.

Most of the features associated to the growing pattern of the $Li^+(H_2O)_n$ are also apparent from Figure 1. We observe in this figure that all clusters up to $n = 20$ present a set of small distances associated to the first solvation shell; the number of water molecules directly coordinated to the ion (*i.e.*, the coordination number, CN) is given in Table 2. In the first solvation shell, all ion-water distances keep essentially at the Li^+-water equilibrium geometry (*i.e.*, ~ 2.0 Å), although larger values with some oscillation arise for $n \geq 14$ in order to accomodate extra water molecules and, hence, increase CN. Indeed, Table 2 shows that, after the completeness of the first solvation shell at $n = 4$, CN keeps as four for most of the clusters, but one obtains global minimum structures with CN=6 and CN=5 for $n = 14$ and $n = 17-19$, respectively. Somehow, this contrasts with our results [16] on the solvation of alkali-metal ions (Na^+, K^+ and Cs^+) with benzene, where the number of solvent molecules that are directly coordinated with the ion keeps the same value as the cluster grows up.

It is interesting to observe in Figure 2 that Li^+ is localized in a peripheral

position in relation to the center of the structure for most of the $Li^+(H_2O)_n$ clusters; as previously pointed out [36], this result is in agreement with molecular dynamics simulations [68]. Only for $n = 2-4$ and 6, the ion occupies the center of the cluster, which is due to the strong influence of Li^+ that is able to "break" the structure of the solvent to originate the first solvation shell. Such "structure-breaking" effect is attenuated beyond the first solvation shell, since the competition between the hydrogen-bond network and the ion-solvent most favorable orientation becomes more relevant, and tends to favor the former, as more water molecules are added to the cluster. This competition is particular evident for $n = 14$ and 15 (see Figure 2). In the former, the ion tends to occupy a more central position, thus favoring the ion-solvent interaction (see below) and the increase of CN to six (as mentioned above); clearly, this behavior is associated with the "structure-breaking" effect, which has been already noticed for $Na^+(H_2O)_n$ clusters [33, 45]. For $n = 15$, the ion occupies now the most off-center position observed for the present set of $Li^+(H_2O)_n$ clusters, which leads to increase significantly the number of H-bonds (see below) with CN=4, and hence showing a weaker "structure-breaking" effect.

Additionally, Figure 1 shows that there is a more clear distinction, in terms of $O - Li^+$ distance, between water molecules in the first two solvation shells than among the more external ones. For example, a first molecule arises in the third solvation shell for $n = 9$, but the corresponding $O - Li^+$ distance is only ~ 0.4 Å greater than for the $n = 8$ most external water molecule which is still located in the second shell. In turn, the $n = 14$ is very compact (with no molecules in the third solvation shell), while the $n = 15$ global minimum is, by contrast, the only one presenting a fourth shell (with ~ 7 Å as the largest $O - Li^+$ distance). This is also apparent from the minimum (for $n = 14$) and the maximum (for $n = 15$) in the curve of the average distance and it is a clear indication of the competition between the ion-water and water-water interaction energies. A similar behavior has been recently observed [16] for Na^+-$(C_6H_6)_{14}$ and Na^+-$(C_6H_6)_{15}$.

We also compare in Table 2 the number of H-bonds for $Li^+(H_2O)_n$ clusters with the corresponding value for the global minima of $(H_2O)_n$ aggregates [46] modeled with the TIP4P potential. As expected, the number of H-bonds diminishes for each $Li^+(H_2O)_n$ cluster in relation to the corresponding aggregate of pure water. The loss of H-bonds due to the presence of Li^+ in the water oscillates as n increases: it varies from a minimum difference of three H-bonds for $n = 7$, 9, 10, and 19 (excluding the special case of $n = 1$, which has only one H-bond) to a maximum difference of five H-bonds for $n = 8$, 12, 14, 16, and 18. In turn, it is apparent from Table 2 that the increase in the number of H-bonds with the addition of a water molecule changes with the size of the cluster, but without showing a well definite pattern. Whilst for most of the $(H_2O)_n$ clusters an additional water molecule leads to form between 1 and 3 extra H-bonds (only for one instance there is no H-bond formation), the corresponding gain in H-bonds for $Li^+(H_2O)_n$ is two in more than 50% of the cases. Due to the competition between water-water and ion-water interactions in $Li^+(H_2O)_n$, a greater variety of situations arises for the increase in the number of H-bonds: one gets zero up to $n = 4$ (*i.e.*, while the first solvation shell is formed) and, also, for $n = 14$ (where the larger CN is obtained); an increase of one H-bond occurs for three clusters, while 3 and 4 arise only once (for $n = 9$ and $n = 15$, respectively). Related to this, we observe in Figure 3 that the ion-solvent contribution for the energy of the clusters increases significantly (becomes more negative) up to the completeness of the first solvation shell, while the solvent-solvent component is zero or slightly positive. Conversely, for $n > 4$ the

solvent-solvent (ion-solvent) contribution tends to increase (to keep approximately constant). Nonetheless, deviations from this general trend arise for n = 14, 17, and 20, where variations in the values of CN are observed (see Table 2).

We now concentrate on the analysis of the new global minimum obtained with the EA for the $Li^+(H_2O)_{17}$ cluster. In Figure 4, we represent two views for both the n = 17 new global minimum (lower panel) and the lowest-energy structure reported by González *et al.* [36] for the corresponding cluster (upper panel). It is apparent from this figure that the lithium ion is located on the surface of the cluster for both structures. However, CN is 5 for the new global minimum, which contrasts with a CN value of 4 for the structure reported by González *et al.* [36]. Thus, the very small energy gap arising for the two structures is due to the competition between the interactions water-water and ion-water; the latter has a major contribution for the new global minimum, while the former stabilizes the second lowest-energy structure. The increase in the ion coordination number leads to reinforce (diminish) the ion-solvent (solvent-solvent) contribution for the energy of the cluster, which is clearly shown in Figure 3 by the peaks in the corresponding ion-water and water-water energy components for n = 17. Nonetheless, the number of H-bonds for the second lowest-energy structure is even smaller than for the global minimum one (*cf.* Table 2). This indicates that the energetic ordering of the solvent-solvent interaction component of the two isomers does not directly correlate with the number of H-bonds; Fanourgakis *et al.* [69] have obtained a similar achivement by performing high-level *ab initio* calculations for different isomers of $(H_2O)_{20}$.

In turn, we performed a re-optimization of the two isomer structures shown in Figure 4 by employing the MP2 *ab initio* method with the aug-cc-pVDZ basis set. The corresponding optimized structures are similar to those in Figure 4, but the isomer with CN=5 resulted to be less stable ($E_{\mathrm{MP2}} = -1304.112436\,E_h$) than the structure with CN=4 ($E_{\mathrm{MP2}} = -1304.121047\,E_h$). Then, we carried out single-point MP2/aug-cc-pVTZ calculations for such optimized geometries and the energies so obtained are $-1305.261048\,E_h$ and $-1305.270918\,E_h$ for CN=5 and CN=4 structures, respectively. At the same levels of theory, the binding energies of the clusters can be calculated as

$$E_{\mathrm{b}}(n) = E_{\mathrm{Li^+-(H_2O)}_n} - E_{\mathrm{Li^+}} - n\,E_{\mathrm{H_2O}} \tag{5}$$

where the three terms are, respectively, the energies of the cluster, and of both isolated ion and water molecule. The calculated difference in the binding energies of the two isomers is $\Delta E_{\mathrm{b}} \sim 23\,\mathrm{kJ\,mol^{-1}}$ ($\Delta E_{\mathrm{b}} \sim 26\,\mathrm{kJ\,mol^{-1}}$) for the aug-cc-pVDZ (aug-cc-pVTZ) basis set, favoring the CN=4 structure over the CN=5 one. To investigate the reason for such reverse in the energy-order of the two structures, we carried out an energy decomposition analysis (EDA). Within the EDA adopted [41], the binding energy is partitioned into the contribution of interaction among water molecules in the hydrated Li^+ complex (ΔE_{S}), and the corresponding water-Li^+ contribution (ΔE_{M}), *i.e*, $E_{\mathrm{b}} = \Delta E_{\mathrm{S}} + \Delta E_{\mathrm{M}}$. The first contribution is given by

$$\Delta E_{\mathrm{S}} = E_{(\mathrm{H_2O})_n^{\#}} - n\,E_{\mathrm{H_2O}} \tag{6}$$

where $E_{(\mathrm{H_2O})_n^{\#}}$ is the energy of an aggregate with n neutral water molecules whose structure is fixed at that of the $\mathrm{Li^+-(H_2O)}_n$ cluster. In turn, the water-Li^+ contribution is calculated by employing the expression:

$$\Delta E_{\mathrm{M}} = E_{\mathrm{Li^+-(H_2O)}_n} - E_{\mathrm{Li^+}} - E_{(\mathrm{H_2O})_n^{\#}} \tag{7}$$

The calculated values of $\Delta E_{\rm b}$, $\Delta E_{\rm S}$ and $\Delta E_{\rm M}$ are given in Table 3 for both aug-cc-pVDZ and aug-cc-pVTZ basis sets. From those values, it follows that, as expected, $\Delta E_{\rm M}$ is larger in magnitude (more negative) for the more coordinated structure. However, such gain in the water-Li^+ energy contribution is achieved at the expense of a less favorable water network ($\Delta E_{\rm S}$ becomes smaller in magnitude), leading to a less negative binding energy; these outcomes are independent of the considered basis set. Thus, the water-water interaction plays a major role in determining the lowest energy configuration for this cluster size.

3.2. $Li^+(CH_3OH)_n$ clusters

The global minimum structures of the $Li^+(CH_3OH)_n$ clusters, as modeled with the OPLS-AA potential, that have been discovered by the EA are represented in Figure 5. A first glance to this figure shows that, like in water, the lithium-ion is preferentially located on the surface of the cluster. Perhaps, such feature becomes more clear by the inspection of Figure 2 (already commented above in the context of the solvation by water), where it is possible to see that the position of Li^+ coincides with the center of the cluster only for $n = 4$. In fact, the first solvation shell is completed with four methanol molecules, *i.e.*, the same pattern as for $Li^+(H_2O)_n$ clusters. In addition, Table 4 shows that the $Li^+(CH_3OH)_n$ global minima keep the same CN=4 up to $n = 9$, and also for $n = 12$. However, nine of the $Li^+(CH_3OH)_n$ clusters have 5 methanol molecules coordinated to Li^+ in the first solvation shell. This increase in the value of CN leads the ion to be localized less off-center than in neighbor clusters with CN=4, which is true for $n = 10$, 11, $13 - 16$ (*cf.*, Figure 2). The global minimum for $n = 20$ corresponds to a peculiar structure with CN=6 (see Figure 5). Nonetheless, as we can see from Table 4, such increase of the CN value does not correspond to a decrease in the number of H-bonds that are formed when an extra methanol is added to the cluster. In contrast to the results reported for the solvation with water, the addition of a methanol molecule leads to the formation of one H-bond for most of the cases; only for 3 instances (*i.e.*, those corresponding to the formation of the first solvation shell) one has no formation of H-bonds upon the addition of a methanol molecule, while in 4 situations the number of H-bonds formed increases to two. Thus, the structural differences observed for the $Li^+(CH_3OH)_n$ as n increases are mainly due to the rearrangement of the first solvation shell to accomodate an additional methanol molecule rather than the larger changes in the H-bond network shown for the solvation with water. Moreover, it is worth noting in Table 4 that, in pure methanol clusters, the formation of one (two) H-bond(s) per methanol added to the structure occurs for 18 cases (only 1 case). Hence, the largest loss of H-bonds due to the presence of Li^+ in methanol is four for $n = 4$. Then, as the first solvation shell is completed, the number of H-bonds in the $Li^+(CH_3OH)_n$ clusters tends to approach the value of the corresponding pure methanol clusters (whose global minima were also obtained with the EA for the OPLS-AA potential); the number of H-bonds of both $(CH_3OH)_n$ and $Li^+(CH_3OH)_n$ clusters becomes coincident for $n \geq 12$, which contrasts with the rather slow convergence noticed in previous subsection for the solvation with water.

We have used the low-energy structures obtained with the EA as starting geometries for a re-optimization at the DFT/B3LYP(6-31+G*) level of theory; these DFT optimizations were extended up to $n = 7$. The lowest-energy structures up to $n = 5$ so obtained are consistent with the corresponding ones reported by Wu *et al.* [40] at the same level of theory. For $n = 6$ and $n = 7$ (the highest value

of n reported by Wu *et al.* [40]), however, our results improve the lowest-energy structures with those given in Ref. [40]. In fact, the global minimum structure of $Li^+(CH_3OH)_7$ displayed in Figure 6 shows two methanol molecules in the second solvation shell, each one establishing two H-bonds with two inner solvent molecules, and another methanol in a third shell; in contrast, the two structures reported in Ref. [40] (that were designated as LIM7I and LIM7II) at the same level of theory are less stable and show only one methanol in the second solvation shell that establishes two H-bonds with two first-shell molecules. Although a more detailed discussion about the structure of the $Li^+(CH_3OH)_6$ is presented in the end of this section, it is already clear that the use of our EA to generate adequate starting geometries for the re-optimization at higher levels of theory is crucial to obtain the lowest-energy structures, especially when dealing with large and fluxional clusters like the present ones.

We have also calculated the frequencies associated to the methanol molecules in the global minima obtained by the DFT/B3LYP/6-31+G* optimization up to $n = 7$. Special attention has been given to the C-O and O-H stretches whose frequencies are represented in Figure 7. As can be seen from Figure 7, the methanol C-O stretch frequencies show a smooth increase (blue shift) of about $50\,cm^{-1}$ from $n = 1$ to $n = 4$, and then continue upwards with a smaller slope of the mean-values curve. However, some scatter in the values of the C-O frequencies is observed for $n \geq 5$, which may be attributed to the methanol-methanol interaction that becomes more important as the first solvation shell is completed. Indeed, as described for neat neutral methanol clusters [25], the hydrogen-bond formation between the methanol molecules occupying different solvation shells is able to produce a blue shift in the C-O stretch. It is worth noting, however, that the C-O frequency is quite affected by the presence of the lithium ion, since it shows a value of $1051\,cm^{-1}$ for the isolated methanol while falling down to $974\,cm^{-1}$ in the $Li^+(CH_3OH)_1$ cluster. Conversely, the O-H stretches keep approximately the same frequency as in the isolated methanol ($3760\,cm^{-1}$) up to $n = 4$ (*i.e.*, the completion of the first solvation shell). For $n = 1$ up to $n = 4$, there is a small shift to the blue by $\sim 25\,cm^{-1}$. However, the mean value of the O-H frequencies decreases (red shifted) when the methanol molecules begin to occupy the second solvent shell (*i.e.*, for $n \geq 5$); also, a strong scatter in the values of the O-H frequencies occurs for $n \geq 5$ (though some O-H frequencies of first-shell molecules keep approximately the value of the isolated methanol), since the methanol molecules in the second solvation shell may experiment different chemical environments. Thus, this behavior reinforces the experimental observation [70] that the vibrational frequencies of O-H stretches in the methanol molecules are mostly determined by solvent-solvent interactions (*i.e.*, due to the formation of hydrogen bonds).

Finally, to further investigate the $Li^+ - (CH_3OH)_6$ cluster, we have used several promising candidates to be the global minimum among the huge number of stationary structures spanning a small energetic window. As mentioned above, such structures obtained with the EA were re-optimized, first, at the B3LYP/6-31+G* level of theory and, successively, with the larger B3LYP/6-311+G** basis set. The hierarchical process ends up with an additional re-optimization where we have employed the aug-cc-pVDZ basis set with the MP2 method; although such level of theory has been considered reliable for hydrogen-bonded systems [71], we have performed single-point MP2/aug-cc-pVTZ calculations to assess the energy order of the isomer structures with further accuracy. This set of successive op-

timizations (or single-point calculations) allowed to reach significant results, but it is important to emphasize at this stage that the choice of various candidate structures to be re-optimized is crucial, since we have no guarantees *a priori* that the OPLS-AA global minimum leads to the *ab initio* or DFT lowest energy; for instance, departing from the global minimum obtained for $Li^+ - (CH_3OH)_6$ cluster with the EA, we could not reach the lowest-energy structure after re-optimizing at the B3LYP/6-31+G* level, and it becomes a saddle-point when relaxing the geometry with the larger B3LYP/6-311+G** basis set. In what follows, we concentrate our discussion on the two lowest-energy structures so obtained for the $Li^+ - (CH_3OH)_6$ cluster. A survey of the energies obtained for the two structures after the optimizations employing DFT and MP2 methods is given in Table 5; it is apparent from this table that the two isomer structures keep the same energetic order for the three levels of theory. The structure labeled as $\mathbf{4+1+1}$ in Table 5 is similar to the lowest-energy cluster obtained by Wu *et al.* [40] (that was designated as LIM6I), and it has 4 methanol molecules in the first solvation shell, one in the second, and another in the third. In turn, the structure designated as $\mathbf{4+2}$ in Table 5 is, indeed, the global minimum in the DFT and MP2 potential energy surfaces, and it shows two methanol molecules in the second solvation shell. To allow a fair comparison with the results of Ref. [40], we represent in Figure 8 the $\mathbf{4+1+1}$ structure and the corresponding infrared spectrum calculated at the DFT(B3LYP/6-31+G*) level of theory. It is clear from this figure that the $\mathbf{4+1+1}$ minimum reproduces the LIM6I structure and its main spectroscopic features (see Figure 2 and Figure 4 of Ref. [40]). Similar data is displayed in Figure 9 for the $\mathbf{4+2}$ minimum which is the most stable structure. It is interesting to notice in these figures that the calculated infrared spectrum of the $\mathbf{4+2}$ structure shows two distinct bands centered at $\sim 990\,cm^{-1}$ and $\sim 1025\,cm^{-1}$, while in the $\mathbf{4+1+1}$ local minimum the two bands are quite mixed with two main peaks at $\sim 1010\,cm^{-1}$ and $\sim 1025\,cm^{-1}$ (in agreement with the calculations carried out in Ref. [40]).

It is worthnoting that Wu *et al.* [40] had attributed the changes in the experimental spectra of $Li^+(CH_3OH)_n$ clusters (for $n \geq 5$) to a combination of charge diffusion and multi-layer solvation effects. Although an unambiguous identification of the different isomers was not possible in Ref. [40], the visual comparison between the vibrational predissociation spectra and the corresponding calculated spectra of various isomers for each cluster size appears to indicate a multi-layer solvation of Li^+ with methanol. In particular for $n = 6$, one of the peaks of the vibrational spectrum for the $\mathbf{4+1+1}$ structure (*i.e.*, the lowest-intensity band in Figure 8) is compatible with the maximum experimentally observed [40] at $\sim 1027\,cm^{-1}$. Nonetheless, we should emphasize that the calculated spectrum of the $\mathbf{4+2}$ global minimum structure shows the highest-intensity band in the frequency region of the experimental maximum (see Figure 9); hence, it is also compatible with the experimental spectrum obtained in Ref. [40] for the $Li^+(CH_3OH)_6$ cluster.

4. Conclusions and final remarks

We have employed a methodology based on EAs to search for low-energy minima of clusters resulting from the microsolvation of the lithium ion with polar solvents that establish important hydrogen-bonds. In particular, the $Li^+(H_2O)_n$ and $Li^+(CH_3OH)_n$ clusters, modeled with commonly used force-field potentials,

were studied up to $n = 20$. Since putative global minima for $Li^+(H_2O)_n$ clusters are available in literature, we could test the performance of our EA to discover the lowest-energy structures for this kind of systems. The EA was able to discover all the global minima up to $n = 20$ and it even discovered a new lowest-energy structure for $Li^+(H_2O)_{17}$. This new structure shows five water molecules in the first solvation shell, while the corresponding number for the second lowest-energy minimum is only four. However, the re-optimization of these two $n = 17$ structures at the MP2/aug-cc-pVDZ level of theory leads to an energy reorder, which has been attributed to the water-water interaction; a similar conclusion is obtained after single-point MP2/aug-cc-pVTZ calculations. Conversely, the application of the same re-optimization process for $Li^+(H_2O)_n$ clusters up to $n = 10$ leads to structures that are similar to those obtained with the EA.

As for the $Li^+(CH_3OH)_n$ clusters modeled with the OPLS-AA potential, putative global minimum structures were obtained up to $n = 20$ with the EA for the first time. For comparing the number of H-bonds established, we have also searched for the global minimum of pure methanol clusters up to n=20. Hence, the number of H-bonds of both $(CH_3OH)_n$ and $Li^+(CH_3OH)_n$ clusters lead for the same value for $n \geq 12$, which contrasts with the rather slow convergence noticed in the microsolvation of Li^+ with water. Although both $Li^+(H_2O)_n$ and $Li^+(CH_3OH)_n$ clusters close the first solvation shell with four solvent molecules, most of the global minima for larger $Li^+(CH_3OH)_n$ show five methanol molecules directly coordinating the ion, while such number is four in the case of the solvation with water. Nonetheless, excluding the small-size clusters, the lithium ion prefers to be located on the surface of the structure for both $Li^+(H_2O)_n$ and $Li^+(CH_3OH)_n$, which is due to the increasing importance of the H-bond network beyond the first solvation shell.

By using the geometries of low-energy minima obtained with the EA for $Li^+(CH_3OH)_n$, we have applied an hierarchical re-optimization to achieve more realistic structures. In this procedure, the structures were successively re-optimized at DFT(B3LYP/6-31+G*) level, followed, then, with the larger B3LYP/6-311+G** basis set and, for the smaller clusters, with the MP2/aug-cc-pVDZ; for $Li^+(CH_3OH)_6$, extra single-point MP2/aug-cc-pVTZ calculations were carried out. It becomes apparent from this work that, due to the more fluxional character of the $Li^+(CH_3OH)_n$ clusters (that show a huge number of stationary configurations within a small energy range), the energy reorder after reoptimization is quite often in comparison with the corresponding $Li^+(H_2O)_n$ aggregates. Because of this, it is usually common to miss low-energy minima and, in particular, the global one, when guided by the chemical intuition one builds starting geometries for being optimized with electronic structure methods. Indeed, by employing the present methodology, we have discovered new global minima structures for both $Li^+(CH_3OH)_6$ and $Li^+(CH_3OH)_7$ that were absent in a previous work [40]. This was confirmed for $Li^+(CH_3OH)_6$ by calculating and comparing the vibrational frequencies in the C-O stretching region; also, the new global minimum (*i.e.*, the $\mathbf{4} + \mathbf{2}$ structure) for $Li^+(CH_3OH)_6$ is compatible with the experimental spectrum [40]. In addition, we noticed that the mean value of the O-H frequencies are shifted to red when the methanol molecules begin to occupy the second solvent shell, which is accompanied by a strong scatter in the single values of the O-H frequencies, because the methanol molecules in the second solvation shell experiment different chemical environments. This reinforces the experimental observation [70] that the vibrational frequencies of O-H stretches in the methanol molecules are mostly determined by solvent-solvent interactions,

mainly due to the formation of H-bonds.

Acknowledgments

This work was supported by Fundação para a Ciência e Tecnologia (FCT), Portugal, under project PTDC/QUI/69422/2006, which is financed by Programa Operacional Factores de Competitividade (COMPETE) of QREN and FEDER programs. We are grateful for the provision of supercomputer time on the Milipeia cluster which is hosted at Laboratório de Computação Avançada, Universidade de Coimbra.

References

[1] J. M. Lisy, Infrared studies of ionic clusters: The influence of Yuan T. Lee, J. Chem. Phys. 125 (2006) 132302.

[2] M. K. Beyer, Hydrated metal ions in the gas phase, Mass. Spectrom. Rev. 26 (2007) 517.

[3] D. J. Miller, J. M. Lisy, Entropic effects on hydrated alkali-metal cations: infrared spectroscopy and ab initio calculations of $M^+(H_2O)_{x=2-5}$ cluster ions for M=Li,Na,K, and Cs, J. Am. Chem. Soc. 130 (2008) 15393.

[4] O. Rodriguez, J. M. Lisy, Infrared spectroscopy of $Li^+(CH_4)_n, n = 1 - 9$, clusters, Chem. Phys. Lett. 502 (2011) 145.

[5] N. R. Walker, R. S. Walters, M. A. Duncan, Frontiers in the infrared spectroscopy of gas phase metal ion complexes, New J. Chem. 29 (2005) 1495.

[6] K. Xu, A. W. Cresce, Li^+-solvation/desolvation dictates interphasial processes on graphitic anode in Li ion cells, J. Mater. Res. 27 (2012) 2327–2341.

[7] S. Varma, S. B. Rempe, Coordination numbers of alkali metal ions in aqueous solutions, Biophys. Chem. 124 (2006) 192.

[8] P. Jena, J. A. W. Castleman, Clusters: A bridge across the disciplines of physics and chemistry, Proc. Nat. Acad. Sci. U.S.A. 103 (2006) 10560–10569.

[9] F. B. Pereira, J. M. C. Marques, T. Leitão, J. Tavares, Analysis of locality in hybrid evolutionary cluster optimization, in: Proceedings of the 2006 IEEE Congress on Evolutionary Computation, Vols. 1-6, CEC, Vancouver, 2006, pp. 2270–2277.

[10] F. B. Pereira, J. M. C. Marques, T. Leitão, J. Tavares, Designing Efficient Evolutionary Algorithms for Cluster Optimization: A Study on Locality, in: P. Siarry, Z. Michalewicz (Eds.), Advances in Metaheuristics for Hard Optimization, Springer Natural Computing Series, Springer, Berlin, 2008, pp. 223–250.

[11] F. B. Pereira, J. M. C. Marques, A study on diversity for cluster geometry optimization, Evol. Intel. 2 (2009) 121–140.

[12] J. M. C. Marques, F. B. Pereira, An evolutionary algorithm for global minimum search of binary atomic clusters, Chem. Phys. Lett. 485 (2010) 211–216.

[13] F. B. Pereira, J. M. C. Marques, Towards an effective evolutionary approach for binary lennard-jones clusters, in: Proceedings of the 2010 IEEE Congress on Evolutionary Computation, CEC, Barcelona, 2010, pp. 1–7.

[14] J. L. Llanio-Trujillo, J. M. C. Marques, F. B. Pereira, An evolutionary algorithm for the global optimization of molecular clusters: Application to water, benzene, and benzene cation, J. Phys. Chem. A 115 (2011) 2130–2138.

[15] J. M. C. Marques, F. B. Pereira, A detailed investigation on the global minimum structures of mixed rare-gas clusters: geometry, energetics, and site occupancy, J. Comput. Chem. 34 (2013) 505–517.

[16] J. M. C. Marques, J. L. Llanio-Trujillo, M. Albertí, A. Aguilar, F. Pirani, Alkali-ion microsolvation with benzene molecules, J. Phys. Chem. A 116 (2012) 4947.

[17] R. H. Leary, Global optima of Lennard-Jones clusters, J. Global Optim. 11 (1997) 35.

[18] J. M. C. Marques, A. A. C. C. Pais, P. E. Abreu, Generation and characterization of low-energy structures in atomic clusters, J. Comput. Chem. (2010) 1495.

[19] J. M. C. Marques, A. A. C. C. Pais, P. E. Abreu, On the use of big-bang method to generate low-energy structures of atomic clusters modeled with pair potentials of different ranges, J. Comput. Chem. 33 (2012) 442–452.

[20] D. J. Wales, M. P. Hodges, Global minima of water clusters $(H_2O)_n$, $n \leq 21$, described by an empirical potential, Chem. Phys. Lett. 286 (1998) 65–72.

[21] B. Hartke, Global geometry optimization of molecular clusters: TIP4P water, Z. Phys. Chem. 214 (2000) 1251–1264.

[22] J. Yin, D. P. Landau, Structural properties and thermodynamics of water clusters: a Wang-Landau study, J. Chem. Phys. 134 (2011) 074501.

[23] S. Shanker, P. Bandyopadhyay, Monte Carlo temperature basin paving with effective fragment potential: an efficient and fast method for finding low-energy structures of water clusters $(H_2O)_{20}$ and $(H_2O)_{25}$, J. Phys. Chem. A 115 (2011) 11866–11875.

[24] S. S. Xantheas, Low-lying energy isomers and global minima of aqueous nanoclusters: structures and spectroscopic features of the pentagonal dodecahedron $(H_2O)_{20}$ and $(H_3O)^+(H_2O)_{20}$, Can. J. Chem. Eng. 90 (2012) 843–851.

[25] U. Buck, F. Huisken, Infrared spectroscopy of size-selected water and methanol clusters, Chem. Rev. 100 (2000) 3863.

[26] G. S. Tschumper, J. S. Gonzales, H. F. Schaefer III, Assignment of the infrared spectra of the methanol trimer, J. Chem. Phys. 111 (1999) 3027.

[27] S. L. Boyd, R. J. Boyd, A density functional study of methanol clusters, J. Chem. Theory Comput. 3 (2007) 54.

[28] J. David, D. Guerra, A. Restrepo, Structural characterization of the $(Methanol)_4$ potential energy surface, J. Phys. Chem. A 113 (2009) 10167.

[29] M. M. Pires, V. F. DeTuri, Structural, energetic, and infrared spectra insights into methanol clusters $(CH_3OH)_n$ for $n = 2-12, 16, 20$. ONIOM as an efficient method of modeling large methanol clusters, J. Chem. Theory Comput. 3 (2007) 1073.

[30] F. Schulz, B. Hartke, Dodecahedral clathrate structures and magic numbers in alkali cation microhydration clusters, ChemPhysChem (2002) 98.

[31] B. Hartke, Structural transitions in clusters, Angew. Chem. Int. Ed. (2002) 1468.

[32] F. Schulz, B. Hartke, Structural information on alkali cation microhydration clusters from infrared spectra, Phys. Chem. Chem. Phys. 5 (2003) 5021–5030.

[33] F. Schulz, B. Hartke, A new proposal for the reason of magic numbers in alkali cation microhydration clusters, Theor. Chem. Acc. 114 (2005) 357–379.

[34] B. Hartke, Global geometry optimization of clusters using genetic algorithms, J. Phys. Chem. 97 (1993) 9973–9976.

[35] S. K. Gregurick, M. H. Alexander, B. Hartke, Global geometry optimization of $(Ar)_n$ and $B(Ar)_n$ clusters using a modified genetic algorithm, J. Chem. Phys. 104 (1996) 2684.

[36] B. S. González, J. Hernández-Rojas, D. J. Wales, Global minima and energetics of $Li^+(H_2O)_n$ and $Ca^{2+}(H_2O)_n$ clusters for $n \leq 20$, Chem. Phys. Lett. 412 (2005) 23–28.

[37] C. J. Weinheimer, J. M. Lisy, Gas-phase cluster ion vibrational spectroscopy of $Na^+(CH_3OH)_{2-7}$, J. Phys Chem. 100 (1996) 15305.

[38] E. M. Cabaleiro-Lago, J. Rodríguez-Otero, An ab initio study of $M^+(CH_3OH)_n$ clusters (M = K, Rb, Cs). Competition between interior and surface structures, J. Phys. Chem. A 106 (2002) 7195.

[39] A. García-Muruais, E. M. Cabaleiro-Lago, J. M. Hermida-Ramón, M. A. Ríos, The study of $A(CH_3OH)_{1-6}$ ($A = Li^+, Na^+$) in the gas phase based on ab initio calculations, analysis of the solvation process, Chem. Phys. 254 (2000) 109.

[40] C.-C. Wu, Y.-S. Wang, C. Chaudhuri, J. C. Jiang, H.-C. Chang, Microsolvation of the lithium ion by methanol in the gas phase, Chem. Phys. Lett. 388 (2004) 457.

[41] K. Hashimoto, T. Kamimoto, Theoretical study of microscopic solvation of lithium in water clusters: neutral and cationic $Li(H_2O)_n$ ($n = 1 - 6$ and 8), J. Am. Chem. Soc. 120 (1998) 3560.

[42] M. Albertí, A. Castro, A. Laganà, M. Moix, F. Pirani, D. Cappelletti, G. Liuti, A molecular dynamics investigation of rare-gas solvated cation-benzene clusters using a new model potential, J. Phys. Chem. A 109 (2005) 2906–2911.

[43] N. Faginas-Lago, F. Huarte-Larrañaga, M. Albertí, On the suitability of the ILJ function to match different formulations of the electrostatic potential for water-water interactions, Eur. Phys. J. D 55 (2009) 75–85.

[44] F. Pirani, S. Brizi, L. F. Roncaratti, P. Casavecchia, D. Cappelletti, F. Vecchiocattivi, Beyond the Lennard-Jones model: a simple and accurate potential function probed by high resolution scattering data useful for molecular dynamics simulations, Phys. Chem. Chem. Phys. 10 (2008) 5489–5503.

[45] B. Hartke, A. Charvat, M. Reich, B. Abel, Experimental and theoretical investigation of microsolvation of Na^+-ions in the gas phase by high resolution mass spectrometry and global cluster geometry optimization, J. Chem. Phys. 116 (2002) 3588.

[46] D. J. Wales, J. P. K. Doye, A. Dullweber, M. P. Hodges, F. Y. Naumkin, F. Calvo, J. Hernández-Rojas, T. F. Middleton, The Cambridge Cluster Database, *http://www-wales.ch.cam.ac.uk/ccd.html*, http://www-wales.ch.cam.ac.uk/CCD.html, 2013. Accessed in May, 2013.

[47] W. L. Jorgensen, J. Chandrasekhar, J. D. Madura, R. W. Impey, M. L. Klein, Comparison of simple potential functions for simulating liquid water, J. Chem. Phys. 79 (1983) 926–935.

[48] W. L. Jorgensen, D. S. Maxwell, J. Tirado-Rives, Development and testing of the OPLS all-atom force field on conformational energetics and properties of organic liquids, J. Am. Chem. Soc. 118 (1996) 11225–11236.

[49] L. X. Dang, Development of nonadditive intermolecular potentials using molecular dynamics: solvation of Li^+ and F^- ions in polarizable water, J. Chem. Phys. 96 (1992) 6970.

[50] J. Åqvist, Ion-water interaction potentials derived from free energy perturbation simulations, J. Phys. Chem. 94 (1990) 8021.

[51] J. Nocedal, Updating quasi-Newton matrices with limited storage, Math. Comp. 35 (1980) 773–782.

[52] K. Deb, H.-G. Beyer, Self-adaptative genetic algorithms with simulated binary crossover, Evol. Comput. 9 (2001) 197–221.

[53] M. W. Schmidt, K. K. Baldridge, J. A. Boats, S. T. Elbert, M. S. Gorgon, J. H. Jensen, S. Koseki, N. Matsunaga, K. A. Nguyen, S. Su, T. L. Windus, M. Dupuis, J. Montgomery, Jr., General atomic and molecular electronic structure system, J. Comput. Chem. 14 (1993) 1347–1363.

[54] K. L. Schuchardt, B. T. Didier, T. Elsethagen, L. Sun, V. Gurumoorthi, J. Chase, J. Li, T. L. Windus, Basis set exchange: a community database for computational sciences, J. Chem. Inf. Model. 47 (2007) 1045–1052.

[55] T. H. Dunning, Jr., Gaussian basis sets for use in correlated molecular calculations. I. The atoms of boron through neon and hydrogen, J. Chem. Phys. 90 (1989) 1007–1023.

[56] R. A. Kendall, T. H. Dunning, Jr., R. J. Harrison, Electron affinities of the first-row atoms revisited. Systematic basis sets and wave functions, J. Chem. Phys. 96 (1992) 6796–6806.

[57] A. D. Becke, Density-functional thermochemistry. III. The role of exact exchange, J. Chem. Phys. 98 (1993) 5648.

[58] C. Lee, W. Yang, R. G. Parr, Development of the Colle-Salvetti correlation-energy formula into a functional of the electron density, Phys. Rev. B 37 (1988) 785.

[59] D. J. Wales, J. P. K. Doye, Global optimization by basin-hopping and the lowest energy structures of Lennard-Jones clusters containing up to 110 atoms, J. Phys. Chem. A 101 (1997) 5111.

[60] J. M. C. Marques, J. L. Llanio-Trujillo, P. E. Abreu, F. B. Pereira, How different are two chemical structures?, J. Chem. Inf. Model. 50 (2010) 2129–2140.

[61] Superimposing Algorithm for the Identification of Chiral Structures, http://apps.uc.pt/mypage/faculty/qtmarque/en/software, 2012. Accessed in May, 2013.

[62] H. W. Kuhn, The hungarian method for the assignment problem, Naval Res. Logistics Quart. 2 (1955) 83–97.

[63] J. Munkres, Algorithms for the assignment and transportation problems, J. Soc. Ind. Appl. Math. 5 (1957) 32–38.

[64] D. Feller, E. D. Glendening, D. E. Woon, M. W. Feyereisen, An extended basis set ab initio study of alkali metal cation-water clusters, J. Chem. Phys. 103 (1995) 3526.

[65] H. M. Lee, P. Tarakeshwar, J. Park, M. R. Kołaski, Y. J. Yoon, H.-B. Yi, W. Y. Kim, K. S. Kim, Insights into the structures, energetics, and vibrations of monovalent cation-$(water)_{1-6}$ clusters, J. Phys. Chem. A 108 (2004) 2949.

[66] I. B. Muller, L. S. Cederbaum, F. Tarantelli, Microsolvation of Li^+ in water analyzed by ionization and double ionization, J. Phys. Chem. A 108 (2004) 5831.

[67] J. S. Rao, T. C. Dinadayalane, J. Leszczynski, G. N. Sastry, Comprehensive study on the solvation of mono- and divalent metal cations: Li^+, Na^+, K^+, Be^{2+}, Mg^{2+} and Ca^{2+}, J. Phys. Chem. A 112 (2008) 12944.

[68] A. V. Egorov, E. N. Brodskaya, A. Laaksonen, The effect of ions on solid-liquid phase transition in small water clusters. A molecular dynamics simulation study, J. Chem. Phys. 118 (2003) 6380.

[69] G. S. Fanourgakis, E. Aprà, S. S. Xantheas, High-level ab initio calculations for the four low-lying families of minima of $(H_2O)_{20}$. I. Estimates of MP2/CBS binding energies and comparison with empirical potentials, J. Chem. Phys. 121 (2004) 2655.

[70] J. M. Lisy, Spectroscopy and structure of solvated alkali-metal ions, Int. Rev. Phys. Chem. 16 (1997) 267.

[71] P. Jurečka, J. Šponer, J. Černý, P. Hobza, Benchmark database of accurate (MP2 and CCSD(T) complete basis set limit) interaction energies of small model complexes, DNA base pairs, and amino acid pairs, Phys. Chem. Chem. Phys. 8 (2006) 1985.

[72] W. Humphrey, A. Dalke, K. Schulten, VMD - visual molecular dynamics, J. Molec. Graphics 14 (1996) 33–38.

Table 1: Energy difference $\Delta E = E_n - E_n^{\mathrm{ref}}$, RMSD [60] between the global minima obtained in the present work (E_n) and those (E_n^{ref}) from [36, 46], and success rate of the EA. Each RMSD value given in square brackets is for the best superposition with the corresponding mirror-image. See the text.

	$Li^+(H_2O)_n$		
n	ΔE/kJ mol^{-1}	RMSD/Å	success rate (%)
1	5.9(-4)[a)]	3.6(-7)	100
2	2.0(-3)	1.6(-6)	100
3	1.2(-3)	0.78 [1.5(-5)]	100
4	-6.9(-3)	6.5(-5)	100
5	-5.8(-2)	5.0(-4)	100
6	-0.1087	6.4(-4)	100
7	-0.1645	7.6(-4)	100
8	-0.2172	8.0(-4)	100
9	-0.2818	8.3(-4)	100
10	-0.3368	0.86 [1.1(-3)]	100
11	-0.3791	1.0(-3)	100
12	-0.4470	1.1(-3)	100
13	-0.4947	1.26 [1.2(-3)]	93
14	-0.5788	1.1(-3)	40
15	-0.6126	1.2(-3)	17
16	-0.6683	1.2(-3)	37
17[b)]	-0.7310	1.22	20
18	-0.8171	1.2(-3)	13
19	-0.8746	1.2(-3)	40
20	-0.9059	0.73 [1.3(-3)]	3

[a)]The following notation is adopted: 5.9(-4) means 5.9×10^{-4}.
[b)]New global minimum structure (CN=5) discovered by the EA. In contrast, $\Delta E = -0.7172$ kJ mol^{-1} for the second lowest-energy minimum (CN=4) obtained by the EA and whose structure matches the GM one reported in [36, 46]

Table 2: Number of hydrogen bonds (HB) and ion-coordination number (CN) for the global minimum structures of $Li^+(H_2O)_n$ clusters. The HB values of the $(H_2O)_n$ global minima are also represented for comparison.

	$(H_2O)_n$	$Li^+(H_2O)_n$	
n	# H-bonds	# H-bonds	CN
2	1	0	2
3	3	0	3
4	4	0	4
5	5	2	4
6	8	4	4
7	9	6	4
8	12	7	4
9	13	10	4
10	15	12	4
11	17	13	4
12	20	15	4
13	21	17	4
14	23	17	6
15	25	21	4
16	28	23	4
17[a)]	29	25	5
18	31	26	5
19	31	28	5
20	34	30	4

[a)]In the case of the Li^+-$(H_2O)_{17}$ structure reported in the CCD [36, 46], the number of H-bonds is 24 and CN=4.

Table 3: Energy decomposition analysis (*cf.* Ref. [41]) for the two lowest-energy structures of Li^+-$(H_2O)_{17}$. All energies (in E_h) were calculated with the MP2 method by employing the aug-cc-pVDZ and aug-cc-pVTZ basis sets. See the text.

	aug-cc-pVDZ			aug-cc-pVTZ		
CN	E_b	ΔE_S	ΔE_M	E_b	ΔE_S	ΔE_M
4	-0.449456	-0.205339	-0.244117	-0.442317	-0.198815	-0.243502
5	-0.440845	-0.175002	-0.265843	-0.432446	-0.167944	-0.264502

Table 4: Number of hydrogen bonds (HB) and ion-coordination number (CN) for the global minimum structures of $Li^+(CH_3OH)_n$ clusters. The HB values of the $(CH_3OH)_n$ global minima are also represented for comparison. See the text.

	$(CH_3OH)_n$	$Li^+(CH_3OH)_n$	
n	# HB	# HB	CN
2	1	0	2
3	3	0	3
4	4	0	4
5	5	2	4
6	6	3	4
7	7	5	4
8	8	7	4
9	9	8	4
10	10	9	5
11	11	10	5
12	12	12	4
13	13	13	5
14	14	14	5
15	15	15	5
16	16	16	5
17	17	17	5
18	18	18	5
19	19	19	5
20	20	20	6

Table 5: Comparison of the DFT and MP2 energies (in E_h) for the two lowest-energy structures of Li^+-$(CH_3OH)_6$. See the text.

	DFT/B3LYP				MP2			
structure	6-31+G*	E_b	6-311+G**	E_b	aug-cc-pVDZ	E_b	aug-cc-pVTZ	E_b
$\mathbf{4+1+1}$	-701.457510	-0.226631	-701.701160	-0.224086	-699.993534	-0.225825	-700.6327071	-0.224442
$\mathbf{4+2}$	-701.460451	-0.229572	-701.704020	-0.226946	-699.997584	-0.229874	-700.636182	-0.227916

ACCEPTED MANUSCRIPT

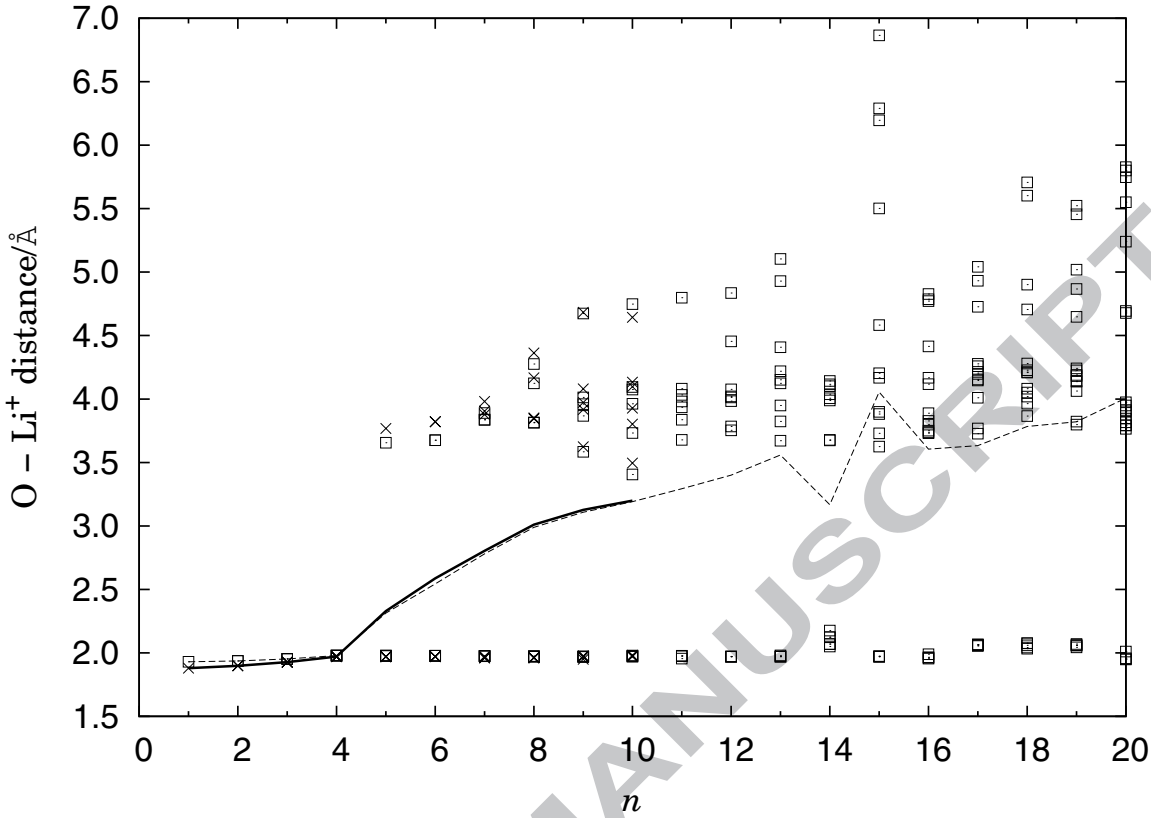

Figure 1: Scatter plot of the distances between the oxygen-atom of the water molecules and the lithium ion as a function of the cluster size. Squares are for the empirical potential model, while the crosses correspond to the *ab initio* structures. The lines link the corresponding average distances.

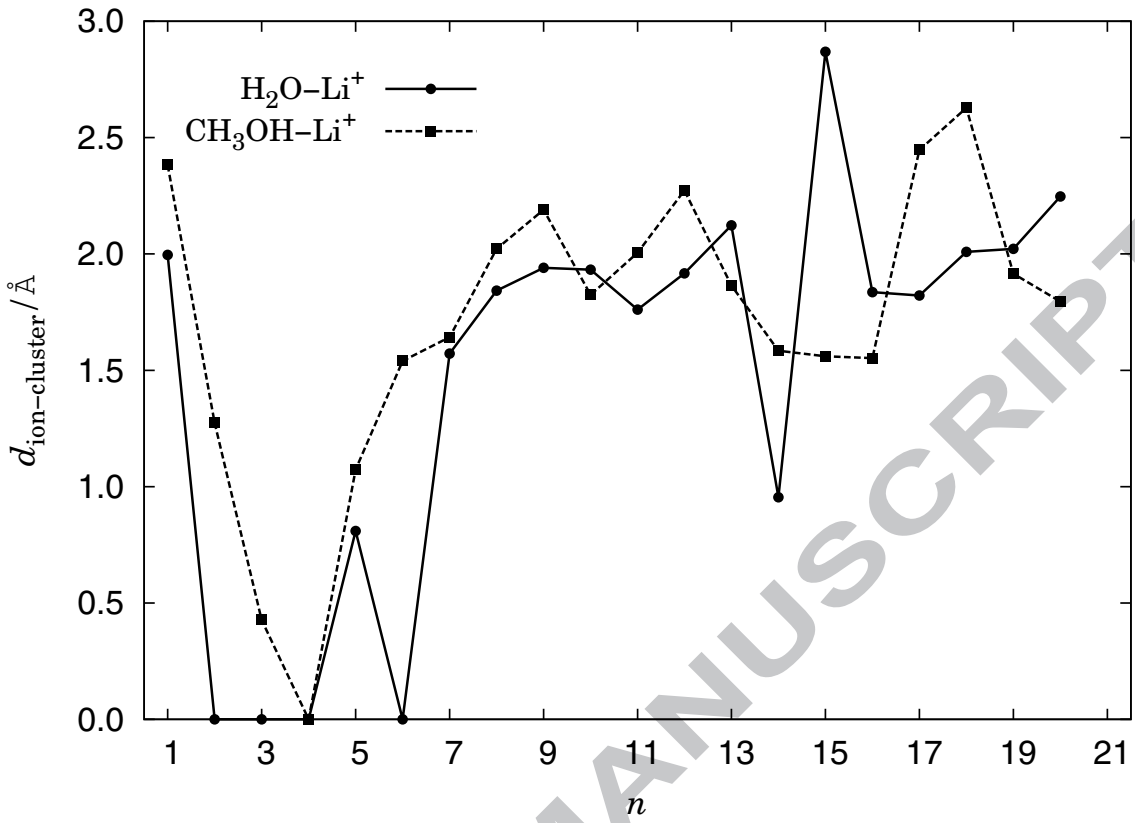

Figure 2: Distance of the lithium ion to the center of the cluster as a function of n. Full line and dots are for $Li^+(H_2O)_n$ global minima, while dashed line and squares correspond to $Li^+(CH_3OH)_n$. See text.

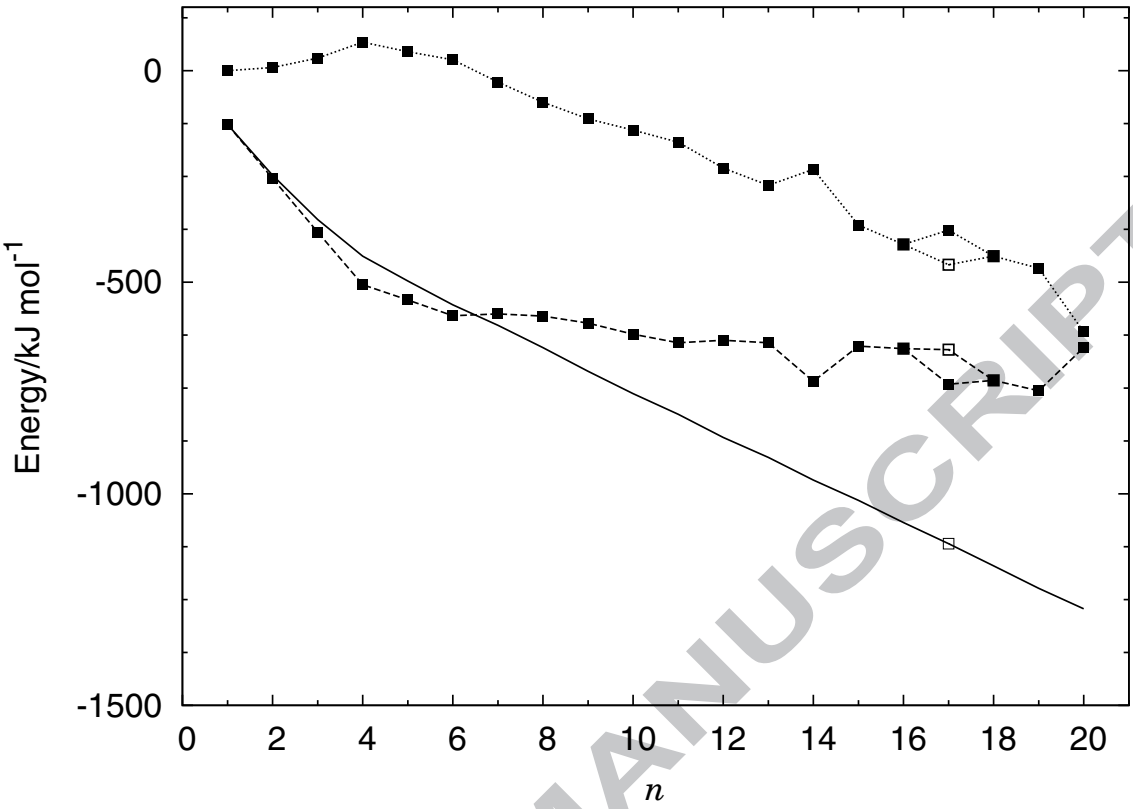

Figure 3: Contributions for the global minima energy of $Li^+(H_2O)_n$ clusters. The energy contribution from the Li^+-water interactions is represented by the dashed line, whereas energy from the water-water pair potentials is shown with a dotted line. Also shown by the solid line is the energy of the global minima. For $n = 17$, the corresponding values for the second lowest-energy minimum (*i.e.*, the putative global minimum in Ref. [36]) are represented by the open squares.

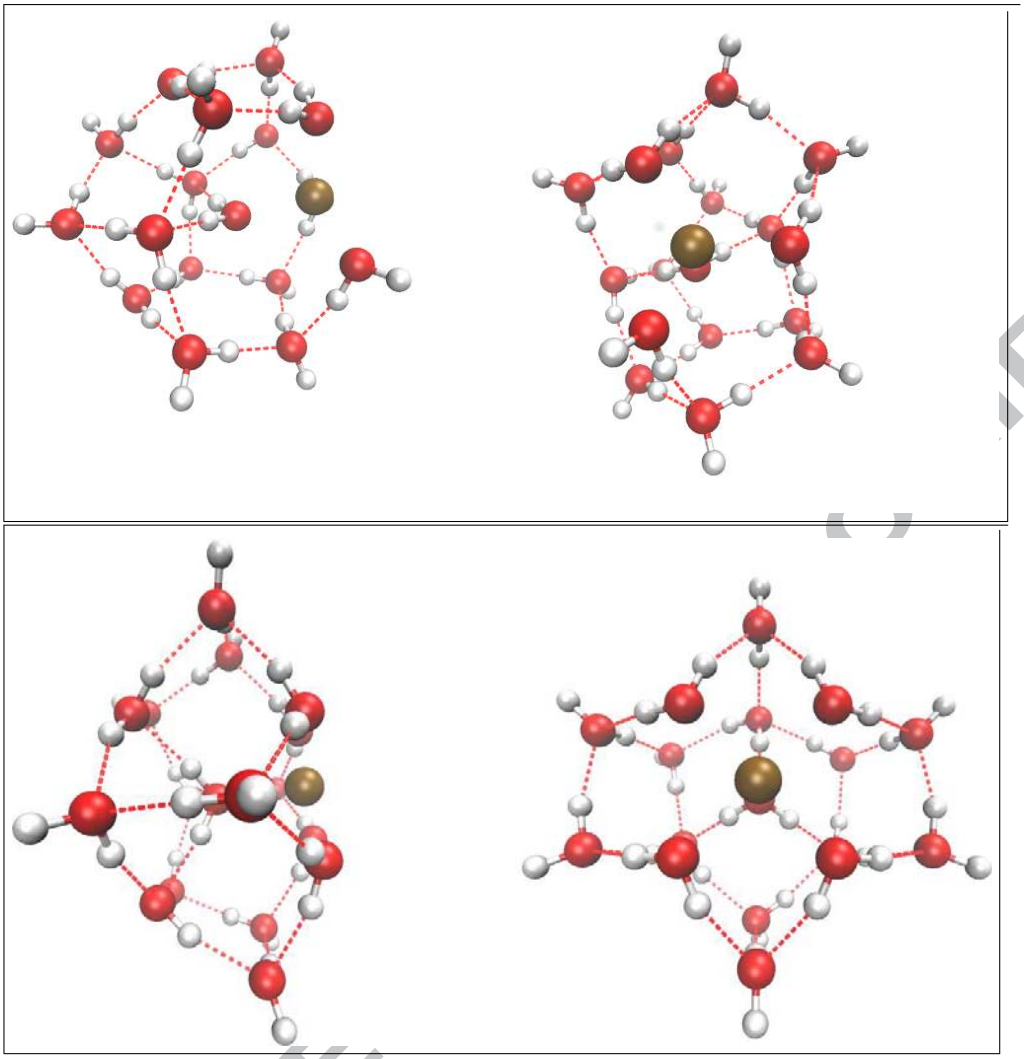

Figure 4: Two views of the second lowest-energy minimum structure for $Li^+(H_2O)_{17}$ (CN=4) whose structure matches the putative global minimum (GM) reported in [36, 46] (upper panel). Two views of the new GM structure for $Li^+(H_2O)_{17}$(lower panel); the new GM has CN=5 and C_s local symmetry (and C_{4v} heavy-atom symmetry, *i.e.*, upon removal of H-atoms on the five waters coordinated by the ion). Plots were produced with VMD program [72].

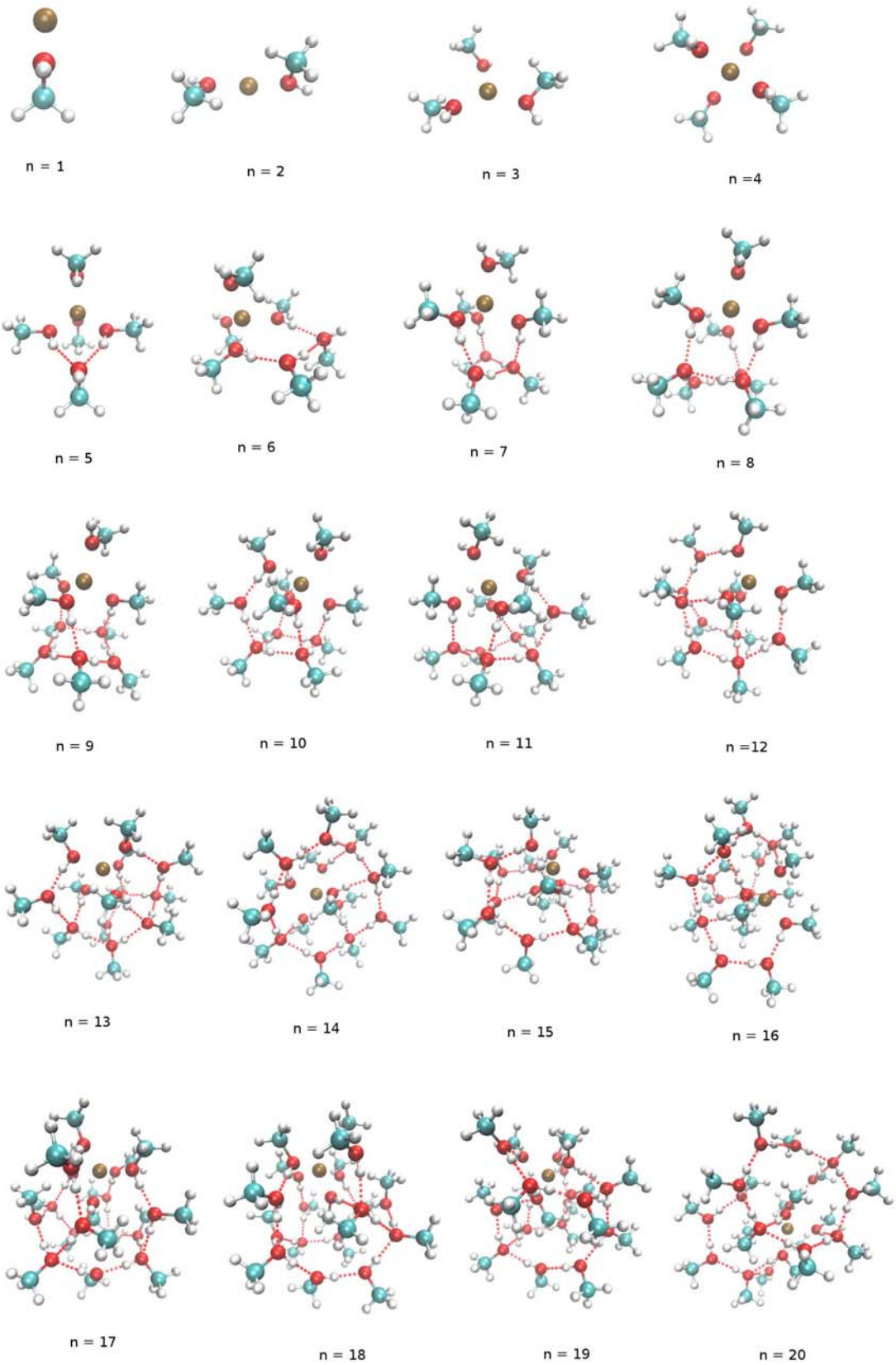

Figure 5: Global minimum structures for $Li^+(CH_3OH)_n$ clusters ($n = 1 - 20$) obtained with the EA for the OPLS-AA potential. Plots were produced with VMD program [72].

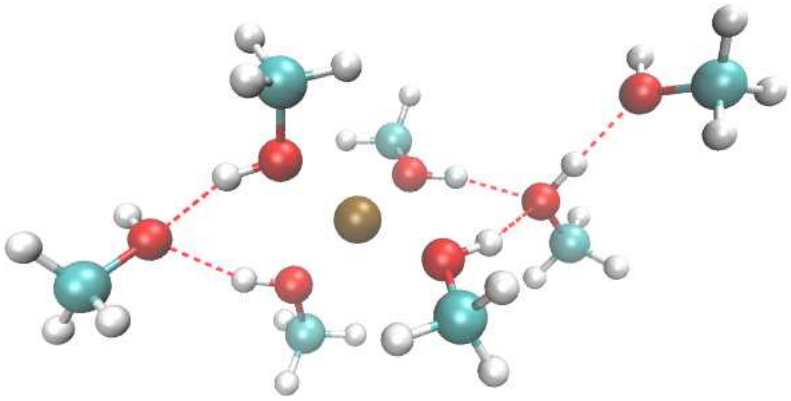

Figure 6: Global minimum structure of the $Li^+(CH_3OH)_7$ cluster obtained by optimization at the DFT(B3LYP/6-31+G*) level of theory. Plot was produced with VMD program [72].

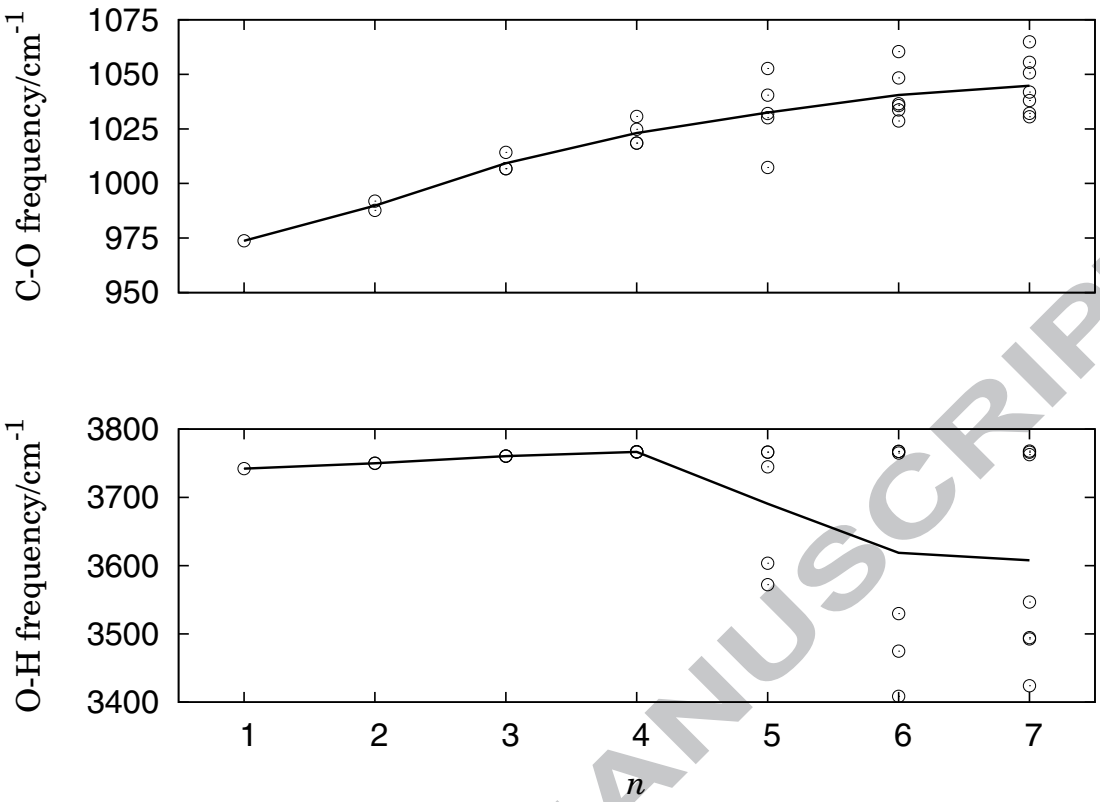

Figure 7: Frequencies of the (a) C-O and (b) O-H stretch modes obtained at DFT(B3LYP/6-31+G*) level for the $Li^+(CH_3OH)_n$ as function of n. Lines link the mean frequency values for each n.

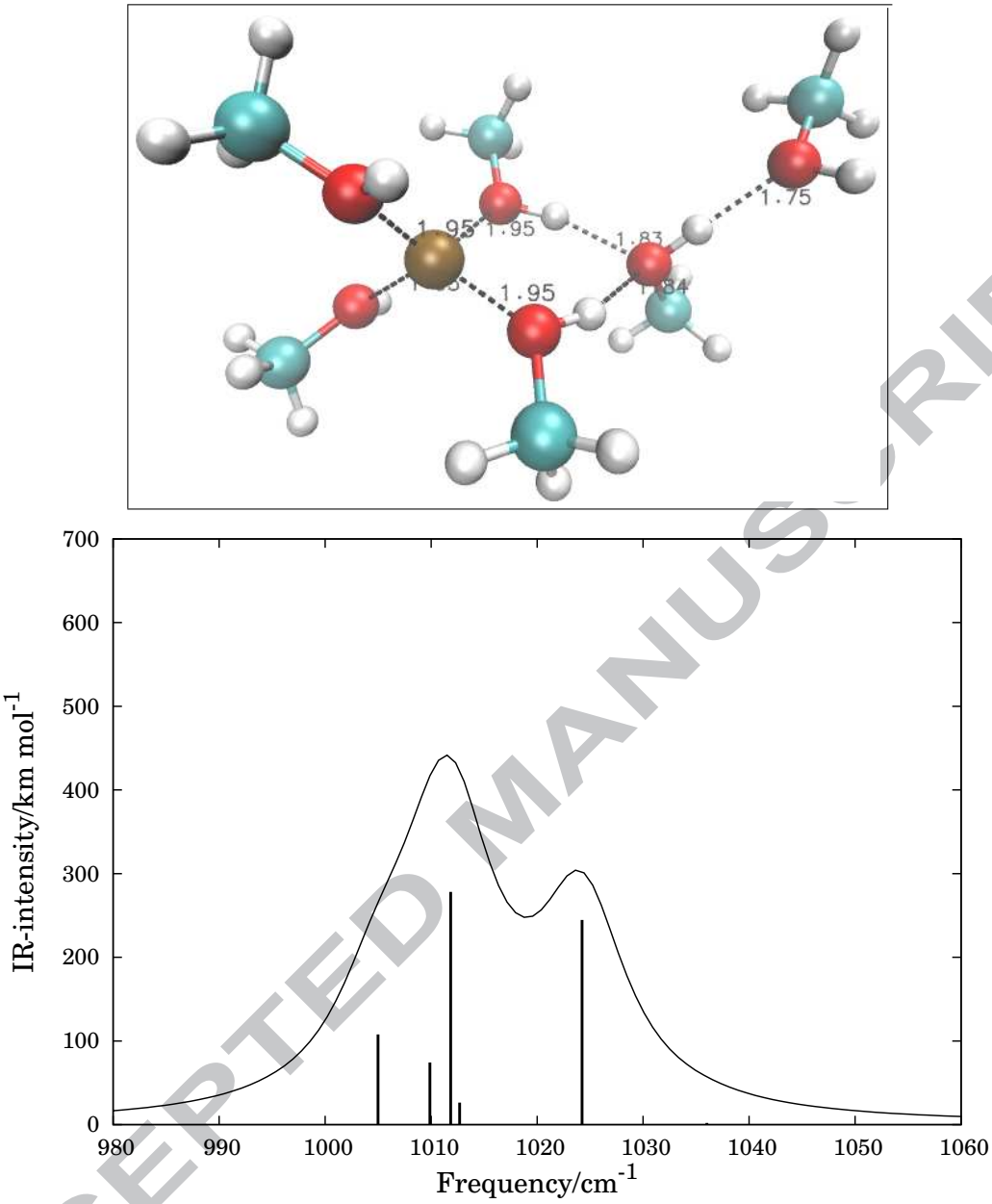

Figure 8: Local-minimum $\mathbf{4}+\mathbf{1}+\mathbf{1}$ structure (upper panel), and the corresponding infrared spectrum (lower panel) obtained by the optimization of the $Li^+(CH_3OH)_6$ cluster at the DFT(B3LYP/6-31+G*) level of theory. The curves in panel (b) correspond to the calculated Lorentzian profiles with FWHM = 10 cm^{-1} for the individual sticks. The calculated CO harmonic vibrational frequencies in cm^{-1} (and corresponding IR frequencies in km/mol), after scaling with the 0.977 factor as in Ref. [40], are: 1004.99 (107.83), 1009.88 (74.27), 1011.85 (278.13), 1012.69 (26.26), 1024.24 (244.60), and 1036.01 (1.94).

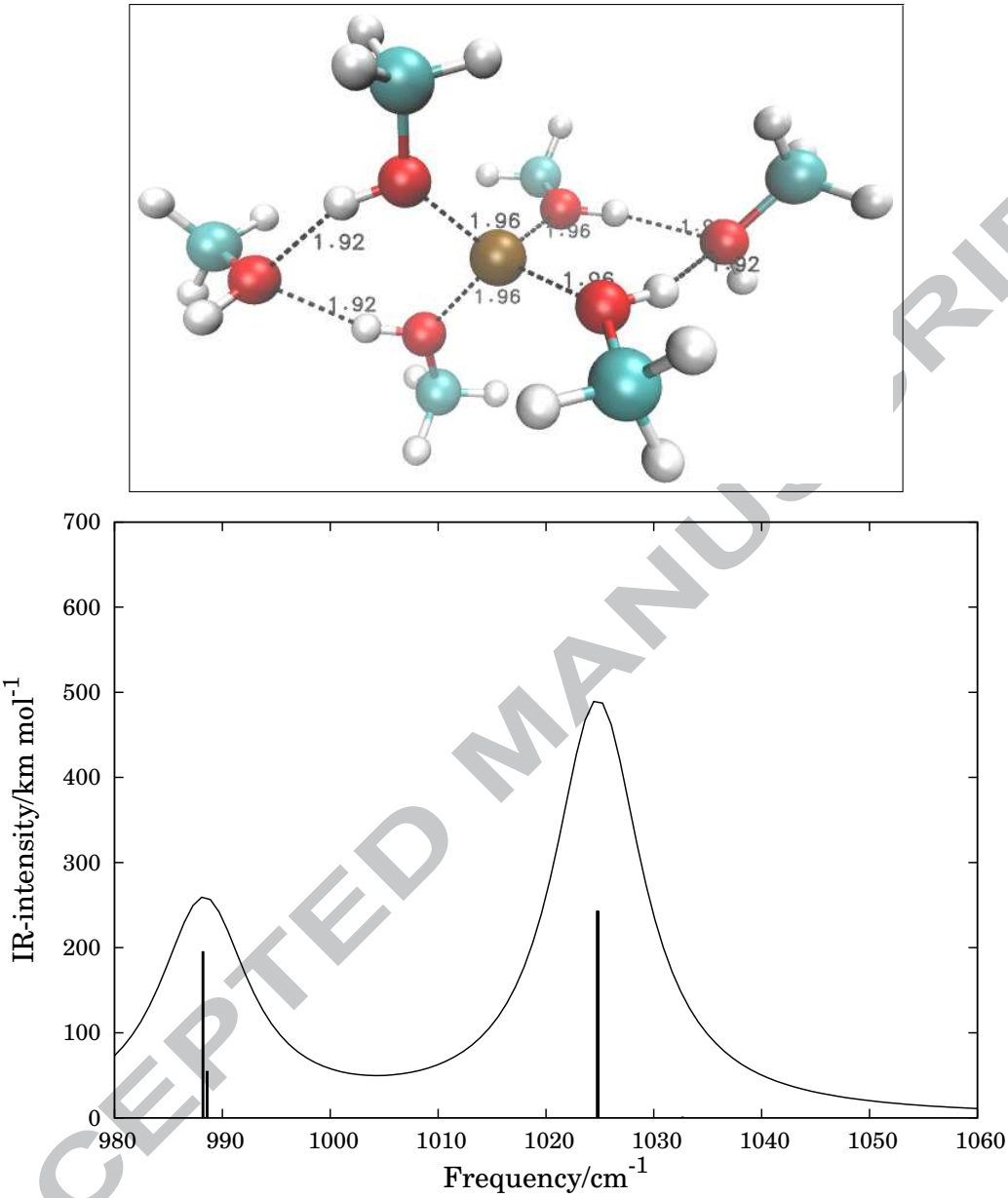

Figure 9: As in Fig. 8, but for the $Li^+(CH_3OH)_6$ global minimum structure (labeled in the text as $\mathbf{4}+\mathbf{2}$). This structure belongs to the C_2 symmetry point group. The calculated CO harmonic vibrational frequencies in cm^{-1} (and corresponding IR frequencies in km/mol), after scaling with the 0.977 factor as in Ref. [40], are: 988.20 (195.82), 988.58 (55.23), 1024.79 (243.23), 1024.80 (243.19), 1032.67 (1.57), and 1039.72(0.03).

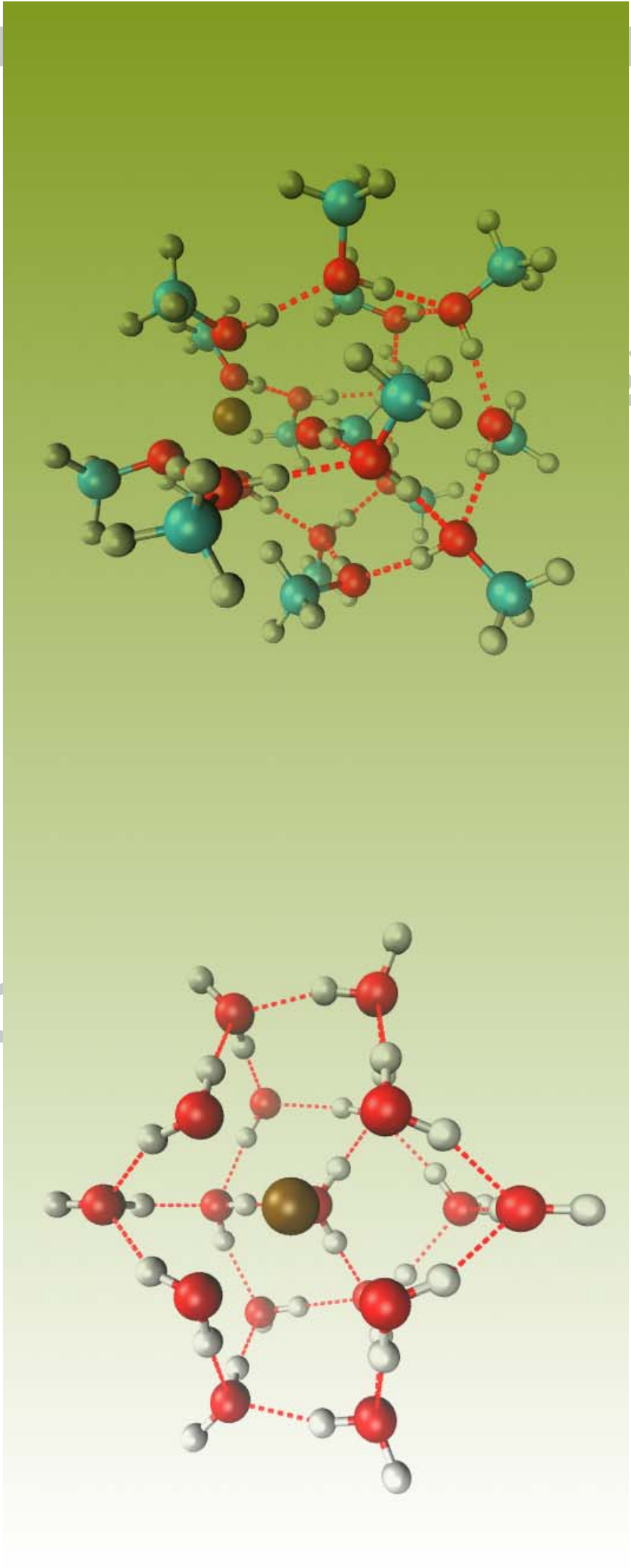

Highlights

- New global minimum discovered for $Li^+(H_2O)_{17}$ with the evolutionary algorithm (EA)
- $Li^+(CH_3OH)_n$ ($n \leq 20$) putative global minima obtained with the EA
- *Ab initio* and DFT re-optimization of the $Li^+(CH_3OH)_n$ clusters leads to energy reorder
- Li^+ is usually located on the surface of both $Li^+(H_2O)_n$ and $Li^+(CH_3OH)_n$ clusters
- New global minimum for $Li^+(CH_3OH)_6$ confirmed by the calculated vibrational spectrum